catalysts

Article

# Au Clusters Supported on Defect-Rich Ni-Ti Oxides Derived from Ultrafine Layered Double Hydroxides (LDHs) for CO Oxidation at Ambient Temperature

**Ayu Takahashi [1], Akihiro Nakayama [1], Toru Murayama [1,2], Norihito Sakaguchi [3], Tetsuya Shimada [1], Shinsuke Takagi [1] and Tamao Ishida [1,*]**

[1] Department of Applied Chemistry for Environment, Graduate School of Urban Environmental Sciences, Tokyo Metropolitan University, 1-1 Minami-osawa, Hachioji, Tokyo 192-0397, Japan
[2] Yantai Key Laboratory of Gold Catalysis and Engineering, Shandong Applied Research Center of Gold Nanotechnology (Au-SDARC), School of Chemistry & Chemical Engineering, Yantai University, 30 Qingquan Road, Yantai 264005, China
[3] Laboratory of Integrated Function Materials, Center for Advanced Research of Energy and Materials, Faculty of Engineering, Hokkaido University, Kita13 Nishi8, Kita-ku, Sapporo, Hokkaido 060-8628, Japan
* Correspondence: tamao@tmu.ac.jp; Tel.: +81-42-677-2845

**Abstract:** Ultrafine layered double hydroxides (LDHs) have abundant hydroxy groups at their edge sites, serving as anchor sites for metal NPs. Furthermore, transformation of ultrafine LDHs into mixed metal oxides (MMOs) generates abundant oxygen vacancies, which are advantageous for $O_2$ activation during Au-catalyzed CO oxidation. We used ultrafine Ni-Ti LDHs with low crystallinity or Ni-Ti MMOs supported on $SiO_2$ onto which Au NPs were deposited by deposition–precipitation (DP) and DP–urea (DPU). The catalytic activity of the Au catalysts was significantly affected by the preparation method, with the highest activity obtained by depositing Au onto LDH/$SiO_2$ by DPU, followed by transformation of LDH to MMO (Au/Ni-Ti MMO/$SiO_2$ (LDH-DPU)). The presence of Au on LDHs affected the transformation of LDHs into MMOs, resulting in LDH-DPU having the greatest number of oxygen vacancies in the $TiO_2$ domain in MMOs. Consequently, the adsorbed or the lattice oxygen on the surface of LDH-DPU can be easily utilized for CO oxidation at low temperatures. Moreover, the catalytic activity of LDH-DPU increased with water vapor concentration up to 100% relative humidity at room temperature, suggesting the potential of Au/Ni-Ti MMO/$SiO_2$ as an air purification catalyst.

**Keywords:** Au catalyst; layered double hydroxide; mixed metal oxide; CO oxidation



**Citation:** Takahashi, A.; Nakayama, A.; Murayama, T.; Sakaguchi, N.; Shimada, T.; Takagi, S.; Ishida, T. Au Clusters Supported on Defect-Rich Ni-Ti Oxides Derived from Ultrafine Layered Double Hydroxides (LDHs) for CO Oxidation at Ambient Temperature. *Catalysts* **2023**, *13*, 1155. https://doi.org/10.3390/catal13081155

Academic Editors: Hongxing Dai and Junhu Wang

Received: 29 June 2023
Revised: 21 July 2023
Accepted: 23 July 2023
Published: 26 July 2023



## 1. Introduction

The catalytic oxidation of harmful CO to $CO_2$ in air at ambient temperature is a fundamental and important process for air purification. In 1987, Haruta et al. reported that Au nanoparticles (NPs) supported on reducible metal oxides exhibited outstanding catalytic activity for CO oxidation at −70 °C [1]. This discovery sparked extensive research on Au catalysts because other metal catalysts, such as Pd and Pt, required higher temperatures exceeding 100 °C. Since then, tremendous efforts have been devoted to the development of highly active Au catalysts. Because the catalytic performance of Au significantly depends on the size of Au NPs and the type of supports, numerous preparation methods have been developed to deposit small Au particles onto various supports [2–4]. Specifically, Au clusters with diameters less than 2 nm are desirable to exhibit high activity. The reaction mechanism of Au-catalyzed CO oxidation has been discussed both experimentally and theoretically [2,4–8]. It is now widely accepted that the active site of Au-catalyzed CO oxidation is Au–support interface. Au works as a CO adsorption sites, and $O_2$ is activated at the oxygen vacancies on the metal oxide supports [4,6–8]. Therefore, reducible metal oxides, such as NiO, $Co_3O_4$, $CeO_2$, and $TiO_2$, have been frequently used as supports for Au NPs.

Recently, single-Au-atom catalysts have attracted increasing interest in order to minimize the use of precious metals [9]. $CeO_2$ [10], $Co_3O_4$ [11], $FeO_x$ [12], and NiO [13] are regarded as suitable supports because single Au atoms can be stabilized at their metal vacancies. However, these single-Au-atom catalysts can be only realized in extremely low loading weights, such as 0.03 wt% of Au [12], except for NiO [13]. This means that a large amount of support is required to exhibit demanding catalytic performance, despite the fact that these metal oxides are classified as rare metals except for $FeO_x$. Therefore, there is a need to minimize the usage of both Au and these rare metal oxides for sustainable development. Although $FeO_x$ is an abundant metal oxide, the $T_{1/2}$ value of $Au_1/FeO_x$, i.e., the temperature of 50% CO conversion, has been reported to be at around 40 °C [12]. Photocatalytic CO oxidation over $Au/TiO_2$ has been also reported, but the working temperature exceeded 60 °C [14].

Despite the abundance of $SiO_2$ on Earth, $SiO_2$ is regarded as an unsuitable support for Au NPs because of the lack of oxygen vacancies and aggregation of Au NPs on $SiO_2$. Conversely, irreducible metal oxides such as $SiO_2$ and $Al_2O_3$ are tolerant of deactivation in CO oxidation under humid air conditions, while $Au/TiO_2$ experiences a decrease in activity in high humidity [15–17]. Thus, there is still room for the development of CO oxidation catalysts that incorporate minimal amounts of Au and rare metals and catalysts capable of functioning at ambient temperature in humid air for applications in air purification.

Layered double hydroxides (LDHs) consist of divalent metal hydroxides with a brucite-layered structure, wherein trivalent metal ions are partially replaced with divalent ones. Many types of LDHs have been synthesized [18]. The chemical formula of LDH is $[M^{2+}{}_{1-x}M^{3+}{}_x(OH)_2][A^{n-}{}_{x/n}\cdot yH_2O]$, where the anion ($A^{n-}$) and water molecules are intercalated to compensate for the positive surface charge. LDHs have interesting features such as a solid base, anion exchange ability, and transformation into mixed metal oxides (MMOs). Natural LDHs, known as hydrotalcite ($[Mg_{0.75}Al_{0.25}(OH)_2][(CO_3{}^{2-})_{0.125}\cdot 0.5H_2O]$), have been used as supports for Au. Because the hydroxyl groups at the edge sites of LDHs are more basic, Au tends to be initially deposited at the edge sites on Mg-Al LDHs, resulting in the formation of Au clusters at low Au loadings. Subsequently, Au is deposited on the lateral face of the LDH to produce aggregated Au NPs [19]. The size of the LDH affects the generation of defects in LDHs [20], and metal- and oxygen vacancies after transformation into MMOs [21,22]. Zhang et al. transformed ultrafine Ni-Ti LDH particles (<4 nm) into defect-rich Ni-Ti MMOs with abundant $Ni^{3+}$ and $Ti^{3+}$ sites [21]. Thus, Ni-Ti LDH NPs with abundant edge OH groups and Ni vacancies are beneficial for stabilizing small Au particles. In addition, the rich oxygen vacancies on the $TiO_x$ domain derived from the Ni-Ti LDH NPs are expected to efficiently activate $O_2$, leading to high catalytic activity for CO oxidation.

In this study, we attempted to form highly dispersed ultrafine Ni-Ti LDH on $SiO_2$ and deposited Au NPs on the prepared Ni-Ti LDH/$SiO_2$ and Ni-Ti MMO/$SiO_2$. The Au particle size and catalytic activity for CO oxidation varied according to the preparation method and support used (LDH/$SiO_2$ or MMO/$SiO_2$). The deposition of Au onto LDH/$SiO_2$ by deposition–precipitation with urea (DPU) followed by the transformation of LDH into MMO gave the most active catalyst, which was active for CO oxidation at room temperature. On the other hand, deposition–precipitation (DP) of Au onto LDH/$SiO_2$, followed by calcination, resulted in relatively large Au NPs with much lower activity. However, DP is more suitable for the deposition of Au onto MMO/$SiO_2$ to obtain small Au NPs. The presence of Au during calcination affected the transformation of LDHs into MMOs, and the number of Ni- and oxygen vacancies in the resultant ultrafine Ni-Ti MMO varied based on the preparation method. Au/Ni-Ti MMO/$SiO_2$, prepared from LDH/$SiO_2$ followed by calcination, possessed abundant oxygen vacancies in the $TiO_x$ domain, which contributed to its high activity. Consequently, we found that the oxygen vacancies could be generated easily by using ultrafine Ni-Ti LDH. Because Ni-Ti LDHs were highly dispersed on $SiO_2$, the use of Ni could also be reduced. Furthermore, the LDH-DPU catalyst exhibited enhanced activity in CO oxidation even at 4% water concentration, which is equal to 100% relative humidity (RH) at room temperature. The results suggest that Au on ultrafine Ni-Ti MMO/$SiO_2$ can serve as efficient air purification catalysts under high humidity conditions.

## 2. Results and Discussion

### *2.1. Characterization of Ni-Ti LDH/$SiO_2$*

Ni-Ti LDH/$SiO_2$ (Ni/Ti = 4/1 atomic ratio) was prepared through hydrothermal synthesis using $Ni(NO_3)_2{\cdot}6H_2O$ and $TiCl_4$, following previously reported methods [23,24] with minor modification. Subsequently, Ni-Ti LDH/$SiO_2$ was converted to Ni-Ti MMO/$SiO_2$ by calcination in air at 500 °C for 2 h (Scheme 1, upper side). Additionally, bulk Ni-Ti MMO was obtained by preparing pristine Ni-Ti LDH in the absence of $SiO_2$ in the same manner, followed by calcination at 500 °C for 2 h. The powder X-ray diffraction (XRD) patterns of bulk Ni-Ti LDH, Ni-Ti LDH/$SiO_2$, and Ni-Ti MMO/$SiO_2$ (Ni/Ti = 4) are shown in Figure 1a. Zhang et al. prepared Ni-Ti LDH NPs with ~20 nm using a reverse microemulsion method in an organic solvent and reported diffraction peaks at 35 and 60°, which corresponded to the (012) and (110) planes, respectively. Additionally, unassigned peaks were observed at around 25, 38, and 45° [21,24]. For the bulk Ni-Ti LDH, diffraction peaks were observed at 10, 25, 34, and 60°, which are almost in agreement with previous reports [21,24]. The peaks at 10 and 25° were probably attributed to the (003) and (006) planes, respectively, suggesting the typical layered structure of LDHs. The peak at 19° was probably ascribed to a partial formation of β-$Ni(OH)_2$ (ICDD No. 00-014-0117) [25]. The broad peaks indicate that small Ni-Ti LDH crystallites were obtained using hydrothermal method. The XRD peaks corresponding to Ni-Ti LDH were also observed for Ni-Ti LDH/$SiO_2$, together with the halo pattern of amorphous $SiO_2$ at approximately 25°. The broad and weak peaks of Ni-Ti LDH suggest that very small Ni-Ti LDH crystallites were formed on $SiO_2$ and/or that the Ni-Ti LDH on $SiO_2$ had low crystallinity.

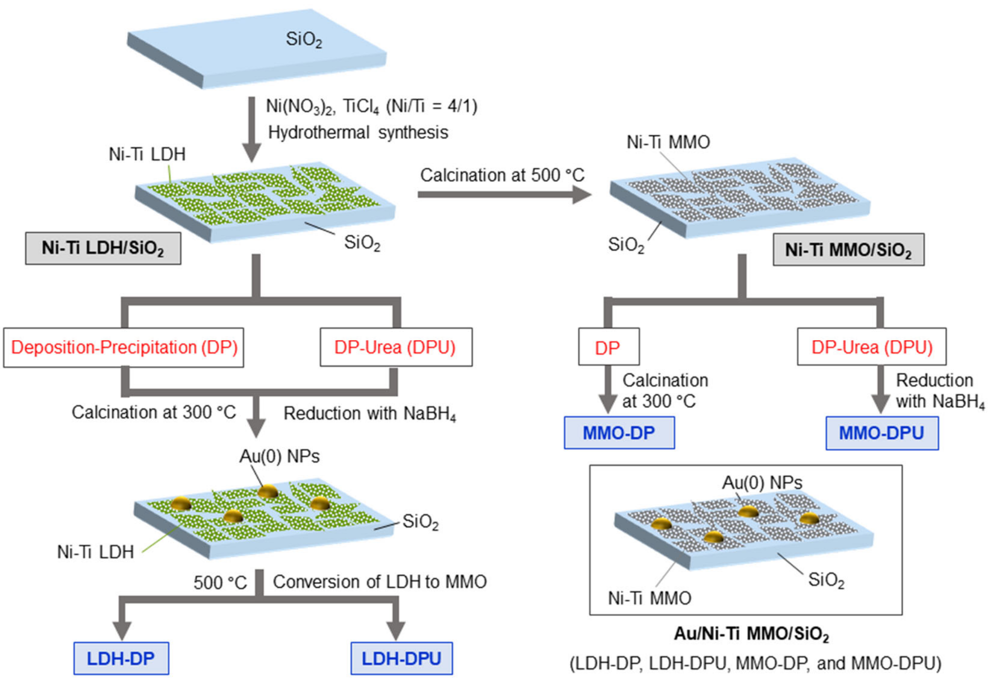


**Scheme 1.** Schematic representation for preparation of four kinds of Au/Ni-Ti MMO/$SiO_2$.

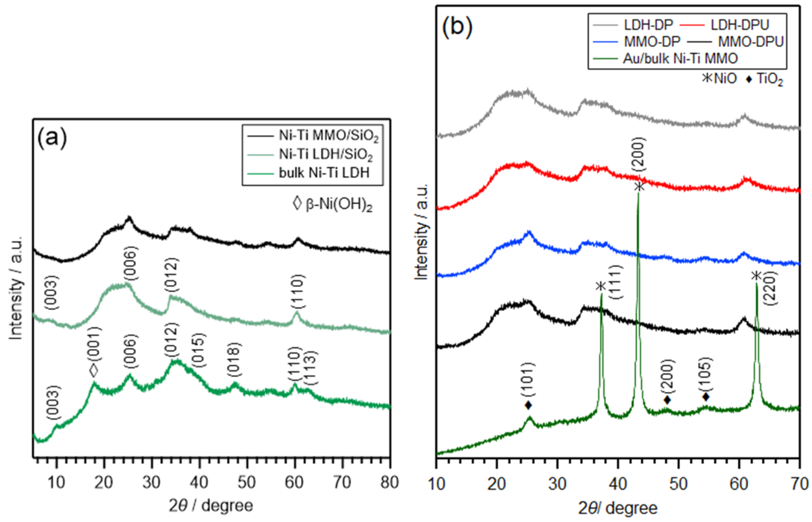


**Figure 1.** (**a**) XRD patterns of bulk Ni-Ti LDH, Ni-Ti LDH/$SiO_2$, and Ni-Ti MMO/$SiO_2$. (**b**) XRD patterns of Au/bulk Ni-Ti MMO and Au/Ni-Ti MMO/$SiO_2$ (LDH-DP, LDH-DPU, MMO-DP, and MMO-DPU).

Thermogravimetric analysis (TGA) was performed to elucidate the transformation of LDHs into MMOs (Figure S1). In the case of bulk Ni-Ti LDH, the weight gradually decreased up to 300 °C, followed by a sharp decline from 300 to 350 °C. These steps coincide with the desorption of the intercalated $H_2O$ and $CO_2$ and the dehydration of hydroxides, respectively [26]. The transformation of LDH to MMO was completed at 400 °C, with a weight loss of 31%, which is consistent with the previous report [21]. These desorption and dehydration steps were shifted to higher temperatures for Ni-Ti LDH/$SiO_2$ (Figure S1), and the transformation into MMO was completed at 550 °C.

### *2.2. Characterization of Ni-Ti MMO/$SiO_2$*

A temperature-dependence study was conducted by varying the calcination temperatures of Ni-Ti LDH/$SiO_2$ within the range of 500 to 900 °C (Figure S2). No obvious change was observed after calcination of Ni-Ti LDH/$SiO_2$ at 500 and 600 °C. However, above 700 °C distinct peaks corresponding to NiO peak at 43° and $NiTiO_3$ peaks at 33 and 35.8° (ICDD No. 00-033-0960) were observed. Calcination below 600 °C produced NiO and $TiO_2$, while $Ni_2TiO_4$ and $NiTiO_3$ were formed above 600 °C [21]. Thus, Ni-Ti LDH/$SiO_2$ was calcined at 500 °C to convert Ni-Ti MMO/$SiO_2$ (Figure 1a).

The XRD pattern of the Au/bulk Ni-Ti MMO showed sharp peaks at 25, 37, 43, and 63°, which were attributed to $TiO_2$ (anatase, ICDD No. 00-021-1272) and NiO (ICDD No. 00-044-1159) (Figure 1b). No obvious change of XRD pattern was observed for Ni-Ti MMO/$SiO_2$, whereas the (003) diffraction at 10° disappeared. In addition, the peaks at 25 and 37° attributed to $TiO_2$ and NiO, respectively, became slightly increased. These results suggest that LDH was converted to MMO, although LDH remaining was not fully ruled out. The broad and weak diffraction peaks suggest that the aggregation of Ni-Ti MMO crystallites could be prevented on $SiO_2$ support during calcination. Scanning electron microscopy (SEM) revealed that Ni and Ti species were highly dispersed on $SiO_2$ (Figure S3). The Ni and Ti loadings were calculated using inductively coupled plasma–atomic emission spectroscopy (ICP-AES) (Table 1). The Ni/Ti atomic ratio was estimated to be 4.8 by ICP-AES, which is almost consistent with the initial Ni/Ti ratio (4/1).

**Table 1.** Physicochemical properties and catalytic activity of Au/Ni-Ti MMO/$SiO_2$.

| Entry | Catalyst | Loading/wt% [1] | | | Au Size [2]/nm | $T_{1/2}$ [3]/°C |
|---|---|---|---|---|---|---|
| | | Au | Ni | Ti | | |
| 1 | LDH-DP | 0.24 | 15 | 2.0 | 4.0 ± 1.5 | 115 |
| 2 | LDH-DPU | 0.28 | 15 | 2.6 | 2.3 ± 2.0 | 10 |
| 3 | MMO-DP | 0.15 | 15 | 2.9 | 1.7 ± 0.5 | 38 |
| 4 | MMO-DPU | 0.3 | 15 | 2.0 | 3.5 ± 1.8 | 191 |
| 5 | Au/Ni-Ti LDH/$SiO_2$ | 0.28 | 15 | 2.6 | 3.5 ± 1.2 | 182 |
| 6 | LDH-DPU-300 | 0.28 | 15 | 2.6 | – | 87 |
| 7 | LDH-DPU-400 | 0.28 | 15 | 2.6 | – | 11 |
| 8 | Au/Ni-Ti MMO/$SiO_2$ (Ni/Ti = 2/1) | 0.25 | 32 | 2.0 | 6.0 ± 2.1 [4] | 65 |
| 9 | Au/bulk Ni-Ti MMO | 0.23 | – | – | 3.2 ± 1.3 | 24 |
| 10 | Au/$TiO_2$ | 0.96 | – | – | 4.1 ± 2.2 | 10–20 |
| 11 | Au/NiO | 0.93 | – | – | – [5] | 57 |
| 12 | Au/$SiO_2$ | 1.00 | – | – | 6.6 ± 2.7 | >300 |
| 13 | Au/$Fe_2O_3$ | 0.81 | – | – | 1.8 ± 0.7 | 36 |

[1] Estimated by ICP-AES. [2] Estimated by HAADF-STEM. [3] The temperature at 50% CO conversion. CO oxidation conditions: 0.1 g of catalyst, 1 vol% CO in air (33.3 mL $min^{-1}$), and space velocity (SV) of 20,000 mL $h^{-1}$ $g_{cat}^{-1}$. [4] The mean diameters of Au particles were estimated by TEM before calcination. [5] Single Au atoms were mainly deposited on NiO [13].

### *2.3. Characterization of Au/Ni-Ti MMO/$SiO_2$*

The deposition of Au NPs to Ni-Ti LDH/$SiO_2$ and Ni-Ti MMO/$SiO_2$ was performed by DP and DPU to give four types of Au catalysts, as shown in Scheme 1. First, Au was deposited on Ni-Ti LDH/$SiO_2$ by DP and DPU, followed by calcination in air at 500 °C to transform LDH to MMO, yielding Au/Ni-Ti MMO/$SiO_2$; the catalysts were denoted as LDH-DP and LDH-DPU, respectively. Alternatively, Au was also deposited on Ni-Ti MMO/$SiO_2$ by DP and DPU; this was followed by the reduction of Au(III) species by air calcination at 300 °C and by reduction with $NaBH_4$, according to the literature [27], giving Au/Ni-Ti MMO/$SiO_2$, denoted as MMO-DP and MMO-DPU, respectively. The initial Au loading was set to 0.3 wt%, and almost 80% of Au was deposited, except for MMO-DP (Table 1). The relatively low actual Au loading for MMO-DP (Au 0.15 wt%) was ascribed to the negatively charged surface (−29 mV) at pH 7, as determined by zeta potential measurement. This surface charge led to electronic repulsion between the MMO/$SiO_2$ and negatively charged Au precursors.

The XRD patterns of four Au/Ni-Ti MMO/$SiO_2$ (Figure 1b) resembled that of Ni-Ti MMO/$SiO_2$ (Figure 1a). No diffraction peaks corresponding to Au were observed owing to low Au loading (Figure 1b). The size of Au particles was estimated by high-angle annular dark-field transmission electron microscopy (HAADF-STEM), and the size distributions are summarized in Table 1 and Figure 2. In Figure 2, a needle-like structure can be observed, which would be ascribed to the layered structure of MMO derived from LDH. The Au particles were highly dispersed on the Ni-Ti MMO/$SiO_2$ of all the catalysts. Although LDH-DP and MMO-DPU gave Au NPs with diameters of 3.5–4.0 nm, Au clusters with diameters of 2.3 and 1.7 nm could be deposited on LDH-DPU and MMO-DP. The Au particle size in the Au/bulk Ni-Ti MMO prepared by DP was estimated to be 3.2 nm (Figure S4). From these results, LDH-DPU and MMO-DP are suitable preparation methods and highly dispersed ultrafine LDH and MMO are beneficial for the deposition of Au clusters.

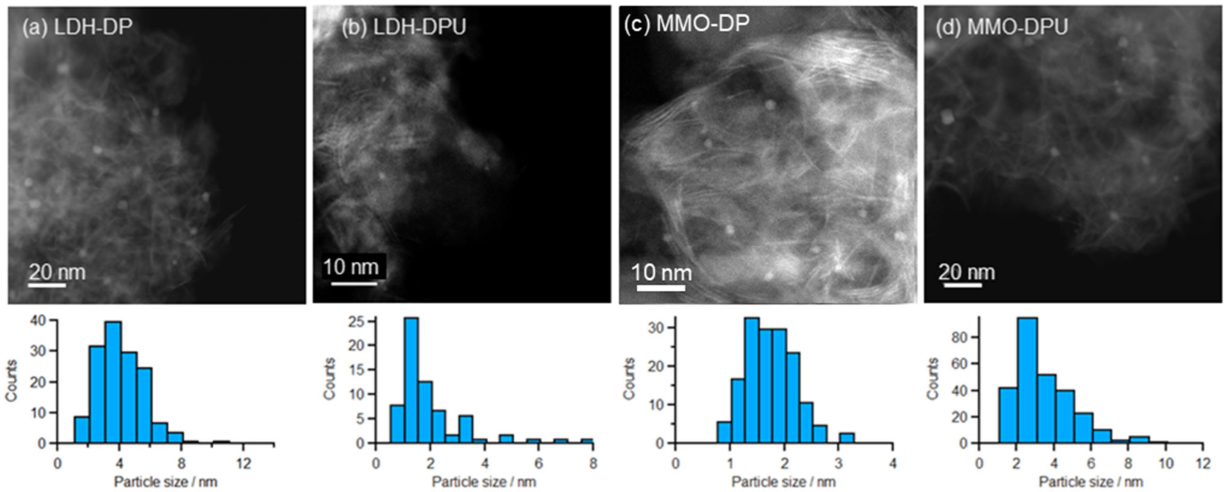


**Figure 2.** TEM images and size distributions of Au/Ni-Ti MMO/$SiO_2$. (**a**) LDH-DP, (**b**) LDH-DPU, (**c**) MMO-DP, and (**d**) MMO-DPU.

Because the $M^{2+}/M^{3+}$ ratio of LDHs can be varied up to 2/1, Ni-Ti LDH with a Ni/Ti ratio of 2/1 was synthesized. Subsequently, Au/Ni-Ti MMO/$SiO_2$ with the Ni/Ti ratio of 2/1 was prepared from NiTi LDH/$SiO_2$ by DPU, followed by calcination to form MMO. However, relatively large Au NPs (6.0 nm) were obtained (Figure S5). The Ni/Ti ratio affected the crystallite size of NiO and $TiO_2$ domains, and a suitable Ni/Ti ratio (4/1) resulted in small Au particles.

### 2.4. Catalytic Activity for CO Oxidation

The catalytic activity of the Au/Ni-Ti MMO/$SiO_2$ for CO oxidation was evaluated using a fixed-bed flow reactor, and the results are shown in Table 1 and Figure 3. The order of catalytic activity is LDH-DPU > MMO-DP > LDH-DP > MMO-DPU (entries 1–4). When compared to LDH-DP and LDH-DPU, LDH-DPU stabilized smaller Au particles with higher loading, exhibiting in higher catalytic activity. In contrast, comparing MMO-DPU and MMO-DP, MMO-DP stabilized smaller Au particles, resulting in higher activity. However, the actual Au loading of MMO-DP was lower than LDH-DPU. As a result, LDH-DPU exhibited the highest catalytic activity and recorded $T_{1/2}$ of 10 °C.

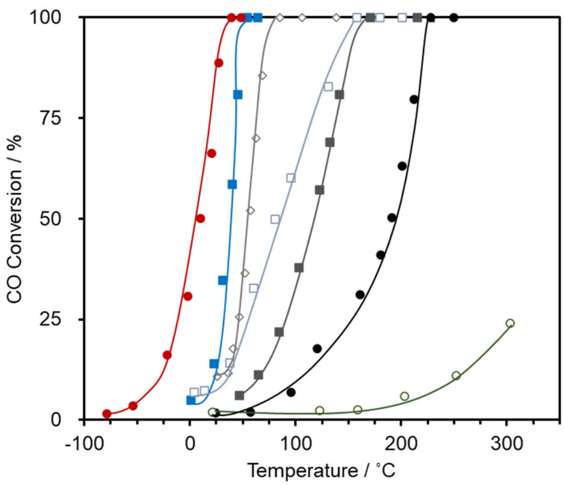


**Figure 3.** Conversion curves for Au-catalyzed CO oxidation. ■: LDH-DP, •: LDH-DPU, ■: MMO-DP, •: MMO-DPU, ◊: Au/$TiO_2$, □: Au/NiO, ○: Au/$SiO_2$. Reaction conditions: 0.1 g of catalyst, 1 vol% CO in air (33.3 mL $min^{-1}$), and space velocity (SV) of 20,000 mL $h^{-1}$ $g_{cat}{}^{-1}$.

In order to reveal the factors for the high activity of LDH-DPU, the transformation of LDH into MMO is discussed. Au/Ni-Ti LDH/$SiO_2$ prepared by DPU followed by the reduction of Au(III) with $NaBH_4$ (entry 5) showed much higher $T_{1/2}$ than LDH-DPU, suggesting that the transformation of LDH into MMO is important for achieving high catalytic activity. The calcination of Au/Ni-Ti LDH/$SiO_2$ at 300 and 400 °C denoted as LDH-DPU-300 and LDH-DPU-400, respectively, was also performed. Although LDH-DPU-400 showed similar activity to that of LDH-DPU, LDH-DPU-300 showed much lower catalytic activity than that of LDH-DPU. Thus, the incomplete transformation of LDH to MMO at 300 °C gave unsatisfactory results (entries 2, 6, and 7).

Next, the dependence of Ni/Ti ratio of Ni-Ti MMO on the catalytic activity was examined. Compared to Ni/Ti = 4/1, Au/Ni-Ti MMO/$SiO_2$ (Ni/Ti = 2/1) showed lower activity than LDH-DPU because of its larger Au NPs (entry 8). Moreover, LDH-DPU exhibited higher activity than Au/bulk Ni-Ti MMO (entries 2 and 9). Given that bulk Ni-Ti MMO has large NiO and $TiO_2$ crystallites, according to XRD (Figure 1), highly dispersed ultrafine NiO and $TiO_2$ domains would work as an efficient support for CO oxidation.

The catalytic activity of the most active LDH-DPU was compared with those of commercially available Au/$TiO_2$, Au/NiO, Au/$SiO_2$, and Au/$Fe_2O_3$ (entries 10–13). Au/$SiO_2$ showed very low activity because $O_2$ could not be activated due to the lack of oxygen vacancies in $SiO_2$ (entry 12). LDH-DPU exhibited higher catalytic activity than Au/NiO, although single Au atoms are major species in Au/NiO (entry 11). It has been reported that inverse NiO-on-Au supported on $SiO_2$ catalysts exhibited high catalytic activity for CO oxidation at room temperature and that the reaction rate was recorded to be 1.74 $mol_{CO}\ g_{Au}^{-1}\ h^{-1}$ [28]. The reaction rate of LDH-DPU was calculated to be 2.32 $mol_{CO}\ g_{Au}^{-1}\ h^{-1}$ at 25 °C, which is superior to the previous report. Au/NiO prepared by double impregnation was also reported to show high activity, and the reaction rate was calculated to be 2.59 $mol_{CO}\ g_{Au}^{-1}\ h^{-1}$ [29]. Although the reaction rate of LDH-DPU was slightly lower than this value, the amount of Ni was lower than the reported Au/NiO. The $T_{1/2}$ of LDH-DPU was almost the same as that of Au/$TiO_2$ whereas the Au loading was smaller (0.3 wt%) than that of 1 wt% Au/$TiO_2$ (entry 10). Moreover, the $T_{1/2}$ of Au/$Fe_2O_3$ was 36 °C, which showed lower activity than LDH-DPU despite the small Au particle size and redox activity of $Fe_2O_3$ (entry 13). From these results, LDH-DPU exhibited the highest catalytic activity based on the amount of Au used.

### 2.5. Evaluation of Oxygen Vacancies on Ni-Ti MMO/$SiO_2$

These CO oxidation results suggest that the catalytic activity significantly varies depending on not only the Au particle size but also the support (LDH or MMO) on which the Au particles are deposited and on the preparation method used. It has been reported that abundant Ni- and O vacancies are formed by the conversion of LDH to MMO, as the size of Ni-Ti LDH decreases [21]. Therefore, the Ni 2p, O 1s, and Ti 2p XPS of the four Au catalysts were measured to evaluate these vacancies, and the results are shown in Figure 4.

Ni $2p_{3/2}$ peaks of LDH-DP, LDH-DPU, MMO-DP, and MMO-DPU were observed at 857.3, 856.7, 858.4, and 857.7 eV, respectively (Figure 4A). The peaks of $Ni^{2+}$, $Ni^{3+}$, Ni oxyhydroxide (NiOOH), and $Ni(OH)_2$ were observed at 854.0–854.4, 855.5–856.3, 856.8–857.7, and 855.4–856.2 eV, respectively [30–35]. When Au was deposited on LDH, the resultant MMO contained $Ni^{2+}$ as the major species, while NiO domains of MMO-DP and MMO-DPU showed a higher energy shift. Although $Ni(OH)_2$ species remaining cannot be fully ruled out, the higher binding energy shift compared to the typical $Ni^{2+}$ of NiO implies the presence of $Ni^{3+}$ species, i.e., rich Ni vacancies, in MMO/$SiO_2$. However, the energy shift did not correlate with the size of the Au particles. Therefore, the size of the Au particles was affected by the preparation method. Accordingly, the smallest Au particle size of MMO-DP was probably due to the low actual Au loading, which prevented aggregation during calcination. For Ni-Ti LDH/$SiO_2$, LDH-DP resulted in larger Au NPs than LDH-DPU, indicating that the aggregation of Au proceeded during calcination at 300 °C before converting LDH into MMO at 500 °C. Compared the samples prepared by DPU, LDH-DPU produced smaller Au particles than MMO-DPU, suggesting that the abundant edge OH groups of ultrafine Ni-Ti LDH were beneficial for stabilizing small Au particles.

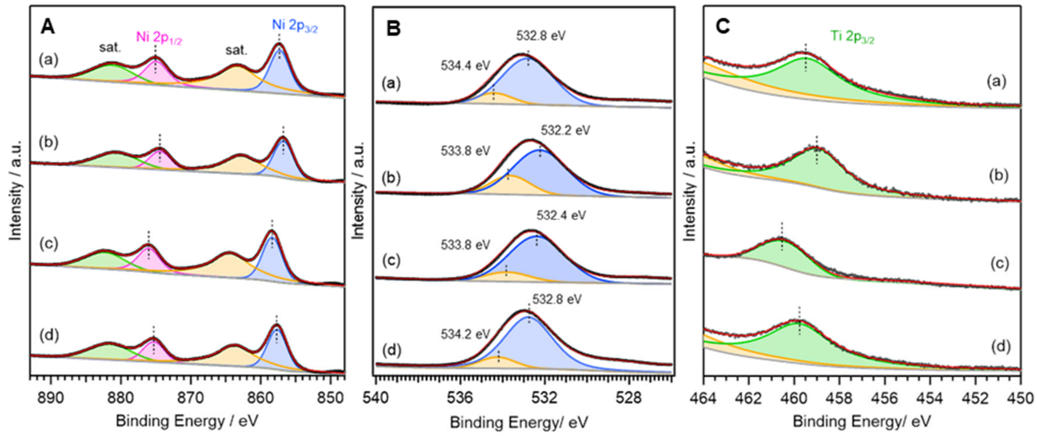


**Figure 4.** (**A**) Ni 2p, (**B**) O 1s, and (**C**) Ti 2p XPS spectra of Au/Ni-Ti MMO/$SiO_2$: (a) LDH-DP, (b) LDH-DPU, (c) MMO-DP, and (d) MMO-DPU.

The presence of oxygen vacancies was evaluated by O 1s and Ti 2p XPS. As shown in Figure 4B, the major O 1s peak was observed at 532.2–532.8 eV corresponding to the lattice oxygen of $SiO_2$ and MMO. The peak at higher binding energy was observed in the range of 533.8–534.2 eV, which was attributed to the oxygen vacancy on the MMO surface [36,37]. Percentages of the peak area ascribed to the oxygen vacancy were calculated to be 23.7%, 14.6%, 14.2%, and 12.3% for LDH-DPU, MMO-DP, LDH-DP, and MMO-DPU, respectively. The number of the oxygen vacancies of MMO increased particularly for LDH-DPU, and the order of the number of oxygen vacancies was consistent with the catalytic activity order.

Furthermore, Ti 2p XPS was also investigated to discuss the oxygen vacancies of the $TiO_x$ domain. Ti $2p_{3/2}$ peaks of LDH-DP, MMO-DP, and MMO-DPU were observed at 459.4, 460.4, and 459.8 eV, respectively (Figure 4C), which are almost consistent with those of $TiO_2$ [38,39]. In contrast, the Ti $2p_{3/2}$ peak of LDH-DPU shifted toward lower binding energies compared to the other three catalysts, at 458.9 eV. The lower energy shift suggests the presence of $Ti^{3+}$ species, indicating an increase in the number of oxygen vacancies in the $TiO_x$ domain. Thus, LDH-DPU, which was rich in oxygen vacancies, exhibited the highest CO oxidation activity. The TGA diagram shows that the transformation of LDH to MMO shifted to a higher temperature in the presence of Au particles on the LDH. This leads to the suppression of MMO crystal growth, resulting in small MMOs with rich oxygen vacancies.

Au 4f XPS analysis was also measured. The Au $4f_{7/2}$ peaks of LDH-DP, LDH-DPU, MMO-DP, and MMO-DPU were observed at 83.4, 83.5, 83.3, and 83.8 eV, respectively. These values are consistent with those of the $Au^0$ NPs (Figure S6).

Figure 5 depicts the relationships between the mean diameter of Au particles and the catalytic activity for CO oxidation based on the XRD, XPS, TEM, and CO oxidation reactions. To exhibit high activity, both an Au particle size smaller than about 2 nm and rich oxygen vacancies on MMOs were found to be key factors. As a result, LDH-DPU exhibited the highest activity.

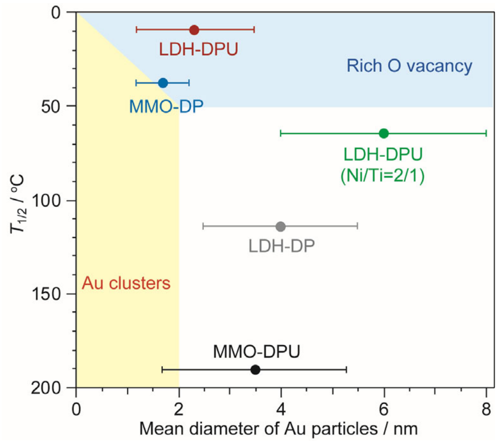


**Figure 5.** Relationships between Au particle size of Au/Ni-Ti MMO/$SiO_2$ and $T_{1/2}$ for CO oxidation.

### 2.6. *Temperature-Programmed Reaction of CO*

To further investigate the difference in the CO oxidation activity with respect to $O_2$ activation, a temperature-programmed reaction of CO (CO-TPR) was performed. Figure 6 shows CO-TPR profiles after pretreatment in air at 250 °C. CO was fed into the sample cell, and the amount of $CO_2$ generated was determined by mass spectrometry. LDH-DPU showed two $CO_2$ desorption peaks at approximately 0 and 100 °C, whereas the other catalysts showed peaks at much higher temperatures. $CO_2$ gradually formed at 20 °C for MMO-DP, whereas only at temperatures above 100 °C for MMO-DPU. The order of the $CO_2$ desorption temperatures was consistent with the $T_{1/2}$ values for CO oxidation.

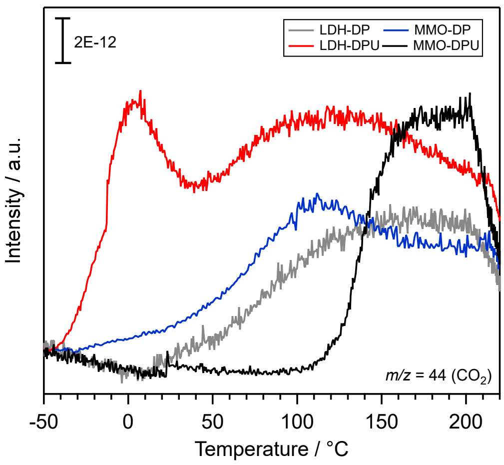


**Figure 6.** CO-TPR profiles of Au/Ni-Ti MMO/$SiO_2$ (LDH-DP, LDH-DPU, MMO-DP, and MMO-DPU). Pretreatment conditions: catalyst (0.1 g), 20 vol% $O_2$ in He (30 mL/min$^{-1}$), 250 °C, 1 h. Measurement conditions: 0.5 vol% CO in He (30 mL/min$^{-1}$), 10 °C/min$^{-1}$.

Behm et al. proposed the Au-assisted Mars–van Krevelen mechanism for CO oxidation over Au/$TiO_2$ [8]. In this mechanism, CO is adsorbed on Au, CO reacts with the surface lattice oxygen of $TiO_2$, and the oxygen vacancy is formed. The lattice oxygen is replenished again by $O_2$, and $CO_2$ finally desorbs. This mechanism is well explained at ambient temperature or above. We reported that the Au-assisted Mars–van Krevelen mechanism for Au/ZnO-catalyzed CO oxidation changes at around −20 °C, and that the activation of weakly adsorbed $O_2$ molecules is critically important for CO oxidation at low temperature [40]. According to these reports, it is likely that the lattice oxygen was used for CO oxidation above 30 °C, but that the $CO_2$ desorption peak at 0 °C is related to weakly adsorbed $O_2$ molecules at the oxygen vacancies. Thus, the CO-TPR results suggest that LDH-DPU possessed more active oxygen species on the MMO surface; $O_2$

would be adsorbed on the abundant oxygen vacancies in the $TiO_x$ domain of MMOs; and/or the surface lattice oxygen of MMOs would be more labile owing to the disordered small crystallites.

### *2.7. CO Oxidation in Humid Air*

We examined the dependence of water concentration on Au-catalyzed CO oxidation, because high catalytic activity in humid air at ambient temperature is crucial for catalytic application in air purification. We have reported that the catalytic activity of Au/$TiO_2$ markedly dropped to about half of that in dry conditions, even in the presence of 1% $H_2O$ [15]. However, the catalytic activity of Au/$Al_2O_3$ and Au/$SiO_2$ at room temperature was maintained or increased up to 4% $H_2O$ vapor (ca. 100% RH at 20 °C). As shown in Figure 7, the catalytic activity of LDH-DPU increased with increasing water concentration and was 1.5 times higher at 4 vol% $H_2O$ than that under dry conditions. Thus, LDH-DPU was found to be tolerant to high humidity and is a promising candidate for air purification catalysts.

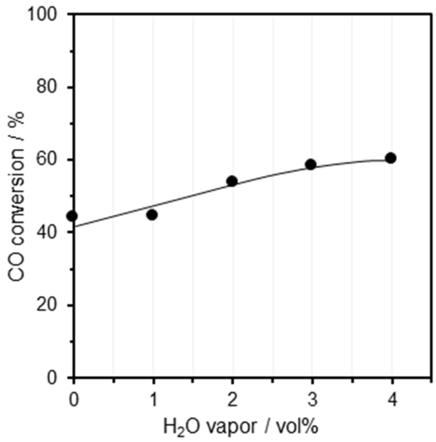


**Figure 7.** Dependence of water concentration on CO oxidation over LDH-DPU at 20 °C. Reaction conditions: catalyst (1.0 wt% Au loading, LDH-DPU, 200 mg), 1 vol% CO in air. $H_2O$ vapor was added, and the total gas flow was set to 50 mL min$^{-1}$. The LDH-DPU was pretreated in $N_2$ (50 mL min$^{-1}$) at 500 °C for 2 h, cooled to room temperature in a flow of $N_2$ (50 mL min$^{-1}$). Subsequently, 1 vol% CO in air containing water vapor (50 mL min$^{-1}$) was passed through the sample cell.

## 3. Materials and Methods

### *3.1. Catalyst Preparation*

#### 3.1.1. Materials

Au/$SiO_2$, Au/NiO, Au/$TiO_2$, and Au/$Fe_2O_3$ (Au 1 wt%) were purchased from Haruta Gold Inc., Tokyo, Japan (https://www.haruta-gold.com/en/) (accessed on 20 July 2023). Aqueous solution of tetrachloroauric acid (0.497 g/L Au) was purchased from Tanaka Kikinzoku Kogyo K.K. and used as received. $SiO_2$ (Q-10) was supplied from Fuji silysia Co., Ltd., Aichi, Japan. Nickel (II) nitrate hexahydrate ($Ni(NO_3)_2 \cdot 6H_2O$: 98%), super-dehydrated toluene (99.5+%), and sodium tetrahydroborate ($NaBH_4$: >95.0%) were purchased from FUJIFILM Wako Pure Chemical Corporation. Titanium (IV) chloride ($TiCl_4$: >99.0%) and urea ($CO(NH_2)_2$: >99.0%) were purchased from Kanto Chemical Co., Inc., Tokyo, Japan (https://www.kanto.co.jp/english/) (accessed on 20 July 2023). Other reagents were commercially available and used without further purification.

#### 3.1.2. Ni-Ti LDH/$SiO_2$

Ni-Ti LDH/$SiO_2$ (Ni/Ti = 4) was prepared using hydrothermal synthesis method according to the literature [23,24] with modifications in the presence of $SiO_2$. $Ni(NO_3)_2$ $6H_2O$ (6 mmol), $TiCl_4$ (1.5 mmol), and urea (15 mmol) were dissolved in 30 mL of distilled water at room temperature, and the solution was stirred at room temperature for 2 h. $SiO_2$ (1.2 g) was added to the solution, and the mixture was transferred to a 50 mL Teflon-lined autoclave and aged at 130 °C for 48 h. The resulting solid was centrifuged, washed with water three times, and dried in air at 80 °C to obtain Ni-Ti LDH/$SiO_2$. The obtained Ni-Ti LDH/$SiO_2$ was calcined in air at 500 °C for 2 h to obtain Ni-Ti MMO/$SiO_2$. Bulk Ni-Ti LDH was prepared in the same manner in the absence of $SiO_2$.

#### 3.1.3. Au/Ni-Ti MMO/$SiO_2$ (LDH-DP and MMO-DP)

Au/Ni-Ti MMO/$SiO_2$ (LDH-DP and MMO-DPU) was prepared by DP. Typically, an aqueous solution of $HAuCl_4$ (10 mM, 0.76 mL) dissolved in distilled water (6.8 mL) was heated to ca. 70 °C, and the pH of the solution was adjusted to 5 by adding 0.1 M NaOH aq. while stirring. A Ni-Ti MMO/$SiO_2$ support was added, and the pH of the suspension was adjusted to 7 by adding 0.1 M NaOH aq. After aging at 70 °C for 1 h, the precipitate was collected by centrifugation, washed five times with water at 40 °C, and dried in air at 80 °C overnight. The resulting solid was calcined in air at 300 °C for 4 h to obtain MMO-DP. Au/Ni-Ti MMO/$SiO_2$ (LDH-DP) was prepared in a similar manner using Ni-Ti LDH/$SiO_2$ as a support, followed by calcination in air at 500 °C for 2 h to convert LDH into MMO, after depositing Au.

#### 3.1.4. Au/Ni-Ti MMO/$SiO_2$ (LDH-DPU and MMO-DPU)

Au/Ni-Ti MMO/$SiO_2$ (LDH-DPU and MMO-DPU) was prepared by DP-Urea according to the literature [27] with minor modifications. For LDH-DPU, an aqueous solution of $HAuCl_4$ ($8.7 \times 10^{-5}$ mol; 10 mM, 870 µL, Au 0.3 wt% initial loading) and 28% ammonia solution (1.2 mL) were dissolved in distilled water (200 mL), and the solution was stirred at room temperature for 4 h. Then, the Ni-Ti LDH/$SiO_2$ support (525 mg) and urea (2.1 g, 35 mmol) were added into the solution. After stirring the suspension at 75 °C for 4 h, the suspension was left overnight at room temperature. The precipitate was collected by centrifugation, washed three times with water at room temperature, and dried in air at 80 °C overnight. The resulting solid (436 mg) was dispersed in anhydrous toluene (109 mL), and $NaBH_4$ (54 mg) was added. The suspension was stirred at room temperature for 2 h. Then, EtOH (33 mL) was added, and the suspension was stirred at room temperature for an additional 6 h. After filtrating and washing with water and ethanol, the solid was dried in air at 80 °C overnight. Subsequently, the solid was calcined in an $N_2$ flow (50 mL $min^{-1}$) at 300, 400, and 500 °C for 2 h at a heating rate of 5 °C $min^{-1}$, to convert LDH to MMO, resulting in LDH-DPU-300, LDH-DPU-400, and LDH-DPU, respectively. Au/Ni-Ti MMO/$SiO_2$ (MMO-DPU) was also prepared by following a similar manner and using Ni-Ti MMO/$SiO_2$ as the support but without calcination in $N_2$ at 500 °C at the final step.

#### 3.1.5. Au/bulk Ni-Ti MMO

Au/bulk Ni-Ti MMO was prepared by DP. The obtained bulk Ni-Ti LDH was converted to bulk Ni-Ti MMO by calcination at 500 °C for 2 h at a ramping rate of 5 °C $min^{-1}$. Subsequently, Au was deposited on bulk Ni-Ti MMO by DP. An aqueous solution of $HAuCl_4$ (25 mM, 0.30 mL) dissolved in distilled water (7.3 mL) was heated to 70 °C, and the pH of the solution was adjusted to 5 by adding 0.1 M NaOH aq. while stirring. The bulk Ni-Ti MMO was added, and the pH of the suspension was adjusted to 7 by adding 0.1 M NaOH aq. After aging at 70 °C for 1 h, the precipitate was collected by centrifugation, washed five times with water at 40 °C, and dried in air at 120 °C overnight. The resulting solid was calcined in air at 300 °C for 4 h to yield Au/bulk Ni-Ti MMO.

### *3.2. Characterization*

XRD patterns were obtained using a Rigaku, MiniFlex with Cu $K\alpha_1$ radiation ($\lambda$ = 0.154 0562 nm). The scan speed and step scan were 5° $min^{-1}$ at 0.02°, respectively. TGA was performed using a HITACHI STA7200. The samples were heated from room temperature to 900 °C at a ramping rate of 10 °C $min^{-1}$ and maintained at 900 °C for 30 min. The actual Au loadings were estimated by ICP-AES using a SPECTRO, CIROS-120, and SHIMADZU, ICPE-9820. The size of the Au particles was estimated HAADF-STEM using a JEOL, ARM-200F NEOARM operating at 200 kV at Tokyo Metropolitan University and an FEI, Titan G2 operating at 300 kV at Hokkaido University. The Au particles were counted more than 150 particles to calculate the mean diameters except for LDH-DPU. For LDH-DPU, it was hard to observe Au particles, and 70 particles were counted. The electronic states of Au, Ni, and Ti were evaluated by XPS using a JEOL, JPS-9010MX with Mg K$\alpha$ radiation. The C 1s peak at 284.6 eV was used for charge correction in the XPS spectra. The CO-TPR was performed on a MicrotracBEL, BELCAT II to investigate the oxygen activation ability of the catalysts. The catalyst sample was pretreated in a flow of 20 vol% $O_2$ in He (30 mL $min^{-1}$) at 250 °C for 1 h and cooled to −100 °C. Then, 0.5 vol% CO in He (30 mL $min^{-1}$) was passed through the catalyst sample at a temperature range of −100–200 °C with a ramping rate of 10 °C $min^{-1}$. The amount of $CO_2$ generated was estimated by mass spectrometry using a MicrotracBEL, BELMASS.

### *3.3. CO Oxidation*

The CO oxidation was performed in a continuous fixed-bed flow reactor. The catalyst sample (0.1 g) was placed in a U-shaped glass reactor and pre-treated in a flow of 20 vol% $O_2$ in $N_2$ (50 mL $min^{-1}$) at 200 °C for 1 h. After cooling to room temperature, 1 vol% CO in air (33.3 mL $min^{-1}$, SV 20,000 mL $h^{-1}$ $g_{cat}{}^{-1}$) was passed through the catalyst bed while heating from room temperature to 300 °C. The CO conversion and $CO_2$ yield were estimated by GC using an Agilent microGC. CO conversion was calculated using the following equation:

$$\text{CO conversion } (\%) = \frac{(\text{CO}_{\text{in}} - \text{CO}_{\text{out}})}{\text{CO}_{\text{in}}} \times 100$$

The effect of water concentration on CO oxidation was evaluated using a MicrotracBEL, BELCAT II equipped with an Agilent microGC. The Au/Ni-Ti LDH/$SiO_2$ catalyst (200 mg) was pre-treated in $N_2$ (50 mL $min^{-1}$) at 500 °C for 2 h. After the pretreatment, the catalyst was cooled to room temperature in a flow of $N_2$ (50 mL $min^{-1}$), and then 1 vol% CO in air containing $H_2O$ vapor (50 mL $min^{-1}$) was fed into the sample cell with water vapor at 20 °C.

## 4. Conclusions

The ultrafine Ni-Ti LDH particles were highly dispersed on $SiO_2$ and converted into small MMO crystallites. Au was deposited on Ni-Ti LDH/$SiO_2$ and Ni-Ti MMO/$SiO_2$ by DP and DPU, and LDHs were finally converted to MMOs. The Au particle size was affected by the preparation method and the support, revealing that the deposition of Au onto LDH by DPU was suitable. The abundant OH groups at the edge sites of LDHs contributed to stabilizing Au clusters. Calcination of LDH/$SiO_2$ after depositing Au by DPU affected the transformation of LDH into MMO, resulting in rich oxygen vacancies in the $TiO_x$ domain. Thus, LDH-DPU exhibited the highest catalytic activity for CO oxidation among the Au/Ni-Ti MMO/$SiO_2$ catalysts and commercially available Au catalysts, despite low Au loading (0.3 wt%). Furthermore, the dispersion of ultrafine Ni-Ti MMO on $SiO_2$ reduced the amount of rare Ni species compared with conventional Au/NiO. In addition, LDH-DPU was active for CO oxidation at room temperature in humid air. These findings will pave the way for the development of highly efficient Au catalysts for air purification.

**Supplementary Materials:** The following supporting information can be downloaded at: https://www.mdpi.com/article/10.3390/catal13081155/s1, Figure S1: TG diagrams of bulk Ni-Ti LDH, Au/Ni-Ti LDH/$SiO_2$, Ni-Ti LDH/$SiO_2$, and $SiO_2$; Figure S2: XRD patterns of Ni-Ti LDH/$SiO_2$ calcined at different temperatures with references, NiO, $TiO_2$, and $NiTiO_3$; Figure S3: SEM-EDS elemental mappings of Ni-Ti LDH/$SiO_2$. (a) SEM, (b) Si, (c) O, (d) Ni, and (e) Ti; Figure S4: TEM image and size distribution of Au particles of Au/bulk Ni-Ti MMO; Figure S5: TEM image and size distribution of Au particles of Au/Ni-Ti LDH/$SiO_2$ (Ni/Ti = 2/1); Figure S6: Au 4f XPS spectra of Au/Ni-Ti MMO/$SiO_2$: (a) LDH-DP, (b) LDH-DPU, (c) MMO-DP, and (d) MMO-DPU.

**Author Contributions:** Conceptualization, T.I.; validation, T.M. and T.I.; investigation, A.T., A.N. and N.S.; data curation, A.T. and A.N.; writing—original draft preparation, A.T. and T. I.; writing—review and editing, T.M., T.S., S.T. and T.I.; visualization, A.T.; supervision, T.I.; project administration, T.I.; funding acquisition, T.I. All authors have read and agreed to the published version of the manuscript.

**Funding:** This research was funded by JSPS and NSFC under the Joint Research Program (JRP with NSFC, Grant Numbers JPJSJRP20191804, MEXT Grant-in-Aid for JSPS KAKENHI (Grant Numbers 19 K05152 and 23H02005), and Izumi Science and Technology Foundation. The research was supported by the Joint Usage/Research Center for Catalysis (Proposal #22DS0077 and 23DS0219) and the JST establishment of university fellowships towards the creation of science technology innovation (Grant Number JPMJFS2139).

**Data Availability Statement:** All relevant data presented in this paper. Catalyst samples are available or not available from the authors.

**Acknowledgments:** We thank Yuki Ono at Tokyo Metropolitan University and Ryo Oota at Hokkaido University for helping with TEM observations.

**Conflicts of Interest:** The authors declare no conflict of interest.

## References

1. Haruta, M.; Kobayashi, T.; Sano, H.; Yamada, N. Novel Gold Catalysts for the Oxidation of Carbon Monoxide at a Temperature Far Below 0 °C. *Chem. Lett.* **1987**, *16*, 405–408. [CrossRef]
2. Ishida, T.; Murayama, T.; Taketoshi, A.; Haruta, M. Importance of Size and Contact Structure of Gold Nanoparticles for the Genesis of Unique Catalytic Processes. *Chem. Rev.* **2019**, *120*, 464–525. [CrossRef] [PubMed]
3. Okumura, M.; Fujitani, T.; Huang, J.; Ishida, T. A Career in Catalysis: Masatake Haruta. *ACS Catal.* **2015**, *5*, 4699–4707. [CrossRef]
4. Ishida, T.; Koga, H.; Okumura, M.; Haruta, M. Advances in Gold Catalysis and Understanding the Catalytic Mechanism. *Chem. Rec.* **2016**, *16*, 2278–2293. [CrossRef] [PubMed]
5. Min, B.K.; Friend, C.M. Heterogeneous Gold-Based Catalysis for Green Chemistry: Low-Temperature CO Oxidation and Propene Oxidation. *Chem. Rev.* **2007**, *107*, 2709–2724. [CrossRef]
6. Fujitani, T.; Nakamura, I. Mechanism and Active Sites of the Oxidation of CO over Au/$TiO_2$. *Angew. Chem. Int. Ed.* **2011**, *50*, 10144–10147. [CrossRef]
7. Widmann, D.; Behm, R.J. Activation of Molecular Oxygen and the Nature of the Active Oxygen Species for Co Oxidation on Oxide Supported Au Catalysts. *Acc. Chem. Res.* **2014**, *47*, 740–749. [CrossRef]
8. Schlexer, P.; Widmann, D.; Behm, R.J.; Pacchioni, G. CO Oxidation on a Au/$TiO_2$ Nanoparticle Catalyst via the Au-Assisted Mars–van Krevelen Mechanism. *ACS Catal.* **2018**, *8*, 6513–6525. [CrossRef]
9. Qiao, B.; Liang, J.X.; Wang, A.; Liu, J.; Zhang, T. Single Atom Gold Catalysts for Low-Temperature CO Oxidation. *Chin. J. Catal.* **2016**, *37*, 1580–1586. [CrossRef]
10. Qiao, B.; Liu, J.; Wang, Y.G.; Lin, Q.; Liu, X.; Wang, A.; Li, J.; Zhang, T.; Liu, J. Highly Efficient Catalysis of Preferential Oxidation of CO in $H_2$-Rich Stream by Gold Single-Atom Catalysts. *ACS Catal.* **2015**, *5*, 6249–6254. [CrossRef]
11. Qiao, B.; Lin, J.; Wang, A.; Chen, Y.; Zhang, T.; Liu, J. Highly Active $Au_1/Co_3O_4$ Single-Atom Catalyst for CO Oxidation at Room Temperature. *Chin. J. Catal.* **2015**, *36*, 1505–1511. [CrossRef]
12. Qiao, B.; Liang, J.X.; Wang, A.; Xu, C.Q.; Li, J.; Zhang, T.; Liu, J.J. Ultrastable Single-Atom Gold Catalysts with Strong Covalent Metal-Support Interaction (CMSI). *Nano Res.* **2015**, *8*, 2913–2924. [CrossRef]
13. Mochizuki, C.; Inomata, Y.; Yasumura, S.; Lin, M.; Taketoshi, A.; Honma, T.; Sakaguchi, N.; Haruta, M.; Shimizu, K.; Ishida, T.; et al. Defective NiO as a Stabilizer for Au Single-Atom Catalysts. *ACS Catal.* **2022**, *12*, 6149–6158. [CrossRef]
14. Pennington, A.M.; Pitman, C.L.; Desario, P.A.; Brintlinger, T.H.; Jeon, S.; Balow, R.B.; Pietron, J.J.; Stroud, R.M.; Rolison, D.R. Photocatalytic CO Oxidation over Nanoparticulate Au-Modifi Ed TiO2 Aerogels: The Importance of Size and Intimacy. *ACS Catal.* **2020**, *10*, 14834–14846. [CrossRef]

15. Dien, L.X.; Ishida, T.; Taketoshi, A.; Truong, D.Q.; Dang Chinh, H.; Honma, T.; Murayama, T.; Haruta, M. Supported Gold Cluster Catalysts Prepared by Solid Grinding Using a Non-Volatile Organogold Complex for Low-Temperature CO Oxidation and the Effect of Potassium on Gold Particle Size. *Appl. Catal. B Environ.* **2019**, *241*, 539–547. [CrossRef]
16. Daté, M.; Okumura, M.; Tsubota, S.; Haruta, M. Vital Role of Moisture in the Catalytic Activity of Supported Gold Nanoparticles. *Angew. Chem. Int. Ed.* **2004**, *43*, 2129–2132. [CrossRef] [PubMed]
17. Saavedra, J.; Pursell, C.J.; Chandler, B.D. CO Oxidation Kinetics over Au/$TiO_2$ and Au/$Al_2O_3$ Catalysts: Evidence for a Common Water-Assisted Mechanism. *J. Am. Chem. Soc.* **2018**, *140*, 3712–3723. [CrossRef]
18. Xu, M.; Wei, M. Layered Double Hydroxide-Based Catalysts: Recent Advances in Preparation, Structure, and Applications. *Adv. Funct. Mater.* **2018**, *28*, 1802943. [CrossRef]
19. Zhang, F.; Zhao, X.; Feng, C.; Li, B.; Chen, T.; Lu, W.; Lei, X.; Xu, S. Crystal-Face-Selective Supporting of Gold Nanoparticles on Layered Double Hydroxide as Efficient Catalyst for Epoxidation of Styrene. *ACS Catal.* **2011**, *1*, 232–237. [CrossRef]
20. Zhao, Y.; Li, B.; Wang, Q.; Gao, W.; Wang, C.J.; Wei, M.; Evans, D.G.; Duan, X.; O'Hare, D. NiTi-Layered Double Hydroxides Nanosheets as Efficient Photocatalysts for Oxygen Evolution from Water Using Visible Light. *Chem. Sci.* **2014**, *5*, 951–958. [CrossRef]
21. Zhao, Y.; Jia, X.; Chen, G.; Shang, L.; Waterhouse, I.N.; Wu, L.; Tung, C.; Hare, D.O.; Zhang, T. Ultrafine NiO Nanosheets Stabilized by $TiO_2$ from Monolayer NiTi-LDH Precursors: An Active Water Oxidation Electrocatalyst. *J. Am. Chem. Soc.* **2016**, *138*, 6517–6524. [CrossRef] [PubMed]
22. Zhao, Y.; Chen, G.; Bian, T.; Zhou, C.; Waterhouse, G.I.N.; Wu, L.; Tung, C.; Smith, L.J.; Hare, D.O.; Zhang, T. Defect-Rich Ultrathin ZnAl-Layered Double Hydroxide Nanosheets for Efficient Photoreduction of $CO_2$ to CO with Water. *Adv. Mater.* **2015**, *27*, 7824–7831. [CrossRef] [PubMed]
23. Ge, X.; Gu, C.; Yin, Z.; Wang, X.; Tu, J.; Li, J. Periodic Stacking of 2D Charged Sheets: Self-Assembled Superlattice of Ni–Al Layered Double Hydroxide (LDH) and Reduced Graphene Oxide. *Nano Energy* **2016**, *20*, 185–193. [CrossRef]
24. Wang, H.; Fan, G.; Zheng, C.; Xiang, X.; Li, F. Facile Sodium Alginate Assisted Assembly of Ni-Al Layered Double Hydroxide Nanostructures. *Ind. Eng. Chem. Res.* **2010**, *49*, 2759–2767. [CrossRef]
25. Cells, D.S.; Qu, Y.; Zhou, W.; Miao, X.; Li, Y.; Jiang, L.; Pan, K. A New Layered Photocathode with Porous NiO Nanosheets: An Effective Candidate for p-Type Dye-Sensitized Solar Cells. *Chem. Asian J.* **2013**, *8*, 3085–3090. [CrossRef]
26. Rathee, G.; Kohli, S.; Panchal, S.; Singh, N.; Awasthi, A.; Singh, S.; Singh, A.; Hooda, S.; Chandra, R. Fabrication of a Gold-Supported NiAlTi-Layered Double Hydroxide Nanocatalyst for Organic Transformations. *ACS Omega* **2020**, *5*, 23967–23974. [CrossRef]
27. Wang, L.; Zhang, J.; Zhu, Y.; Xu, S.; Wang, C.; Bian, C.; Meng, X.; Xiao, F.S. Strong Metal-Support Interactions Achieved by Hydroxide-to-Oxide Support Transformation for Preparation of Sinter-Resistant Gold Nanoparticle Catalysts. *ACS Catal.* **2017**, *7*, 7461–7465. [CrossRef]
28. Xu, X.; Fu, Q.; Guo, X.; Bao, X. A Highly Active "NiO-on-Au" Surface Architecture for CO Oxidation. *ACS Catal.* **2013**, *3*, 1810–1818. [CrossRef]
29. Carabineiro, S.A.C.; Bogdanchikova, N.; Avalos-borja, M.; Pestryakov, A.; Tavares, P.B.; Figueiredo, J.L. Gold Supported on Metal Oxides for Carbon Monoxide Oxidation. *Nano Res.* **2011**, *4*, 180–193. [CrossRef]
30. Li, X.; Patil, K.; Agarwal, A.; Babar, P.; Jang, J.S.; Chen, X.; Yoo, Y.T.; Kim, J.H. $Ni(OH)_2$ Coated CoMn-Layered Double Hydroxide Nanowires as Efficient Water Oxidation Electrocatalysts. *New J. Chem.* **2022**, *46*, 2044–2052. [CrossRef]
31. Xu, J.; Tang, M.; Hu, Z.; Hu, X.; Zhou, T.; Song, K.; Wu, J.; Cheng, J. Standing and Lying $Ni(OH)_2$ Nanosheets on Multilayer Graphene for High-Performance Supercapacitors. *Nanomaterials* **2021**, *11*, 1662. [CrossRef]
32. Liu, G.; Ouyang, X.; Wei, X.; Bao, W.; Feng, X.; Zhang, J. Coupling Interface Construction of $Ni(OH)_2$/$MoS_2$ Composite Electrode for Efficient Alkaline Oxygen Evolution Reaction. *Catalysts* **2022**, *12*, 966. [CrossRef]
33. Liu, A.; Liu, G.; Zhu, H.; Shin, B.; Fortunato, E. Hole Mobility Modulation of Solution-Processed Nickel Oxide Thin-Film Transistor Based on High-k Dielectric. *Appl. Phys. Lett.* **2016**, *108*, 233506. [CrossRef]
34. Chen, Y.S.; Kang, J.F.; Chen, B.; Gao, B.; Liu, L.F.; Liu, X.Y.; Wang, Y.Y.; Wu, L.; Yu, H.Y.; Wang, J.Y.; et al. Microscopic Mechanism for Unipolar Resistive Switching Behaviour of Nickel Oxides. *J. Phys. D Appl. Phys.* **2012**, *45*, 065303. [CrossRef]
35. Shih, Y.; Huang, Y.; Huang, C.P. Electrocatalytic Ammonia Oxidation over a Nickel Foam Electrode: Role of $Ni(OH)_{2(s)}$-$NiOOH_{(s)}$ Nanocatalysts. *Electrochim. Acta* **2018**, *263*, 261–271. [CrossRef]
36. Wang, Z.; Lin, R.; Huo, Y.; Li, H.; Wang, L. Formation, Detection, and Function of Oxygen Vacancy in Metal Oxides for Solar Energy Conversion. *Adv. Funct. Mater.* **2022**, *32*, 2109503. [CrossRef]
37. Ali, H.; Vandevyvere, T.; Lauwaert, J.; Kumar, S.; Saravanamurugan, S.; Thybaut, J.W. Impact of Oxygen Vacancies in Ni Supported Mixed Oxide Catalysts on Anisole Hydrodeoxygenation. *Catal. Commun.* **2022**, *164*, 106436. [CrossRef]
38. Wang, S.; Cai, J.; Mao, J.; Li, S.; Shen, J.; Gao, S. Defective Black $Ti^{3+}$ Self-Doped $TiO_2$ and Reduced Graphene Oxide Composite Nanoparticles for Boosting Visible-Light Driven Photocatalytic and Photoelectrochemical Activity. *Appl. Surf. Sci.* **2019**, *467–468*, 45–55. [CrossRef]

39. Nawaz, R.; Kait, C.F.; Chia, H.Y.; Isa, M.H.; Huei, L.W.; Sahrin, N.T. Synthesis of Black-$TiO_2$ and Manganese-Doped $TiO_2$ Nanoparticles and Their Comparative Performance Evaluation for Photocatalytic Removal of Phenolic Compounds from Agro-Industrial Effluent. *J. Nanopart. Res.* **2021**, *23*, 263. [CrossRef]
40. Fujita, T.; Ishida, T.; Shibamoto, K.; Honma, T.; Ohashi, H.; Murayama, T.; Haruta, M. CO Oxidation over Au/ZnO: Unprecedented Change of the Reaction Mechanism at Low Temperature Caused by a Different $O_2$ Activation Process. *ACS Catal.* **2019**, *9*, 8364–8372. [CrossRef]